A boundary elements only solution method for 3D micropolar elasticity

Gaël Pierson, Richard Kouitat-Njiwa, Pierre Bravetti

A boundary elements only solution method for 3D micropolar elasticity

Pierson Gaël [a,*] ; Richard Kouitat-Njiwa [a] ; Pierre Bravetti [a]

*Corresponding Author

[a] Institut Jean Lamour, Université de Lorraine, 2 allée André Guinier, 54011 Nancy, France.

Email adress: gael.pierson@univ-lorraine.fr (Pierson Gaël)

richard.kouitat@univ-lorraine.fr (Kouitat Richard)

pierre.bravetti@univ-lorraine.fr (Bravetti Pierre)

Abstract

Micropolar elasticity belongs to the class of so-called multi-fields problems. The numerical solution of the associated field equations by the pure boundary element method (BEM) is available only for some 2D geometries. A judicious combination of the local point interpolation method with the pure BEM leads to a pure BEM solution procedure of 3D problems. The effectiveness of the approach is demonstrated on some examples including indentation. A first analysis of the impact of the microstructure on the macroscopic response is presented.

Keywords: boundary element, local point interpolation, micropolar elasticity, indentation

1- Introduction

The concept of micropolar elasticity or Cosserat elasticity was first introduced by the Cosserat brothers Eugène and François, (Cosserat and Cosserat, 1909) at the end of the 18th century, who took into account the microstructure of materials in a quasi-homogeneous description. This description is part of the generalized microcontinuum fields of Eringen ((Eringen, 1999a), Green (Green et al., 1965), Mindlin (Mindlin and Tiersten, 1962) during the sixties. The materials that can be described in the framework of generalized microcontinuum mechanics are numerous and various. As examples one can mention, granular materials such as minerals (Diepolder et al., 1991) or certain metals (Diebels, 2000), liquid crystals or the hard tissues that make up the body of living beings (Park and Lakes, 1986).

At the present time the micropolar media are applied to the description of different media. In the field of electromagnetism one can mention the work of (Maugin, 1988) (Eringen, 1990) . The model is also applied to porous and granular mediae.g. (Lakes, 1986) (Ehlers, 1997) (Diebels, 2002)

(Goddard, 2008) and even in the field of living tissues like bones e.g. (Park and Lakes, 1986) (Ramezani et al., 2009) (Altenbach and Eremeyev, 2009).

In micropolar elasticity, the field equations associated with a given problem allow analytical solutions only for "simple" geometries and stimuli. Generally, we will look for a numerical solution. Different numerical methods have been developed to deal with solid mechanic problems. The most common is the popular and powerful finite element method (FEM) which has been applied to solve micropolar elasticity problems, mainly in the 2D context (Li and Xie, 2004; Ramezani et al., 2008). The development of special 3D finite element in this context has been recently been presented by Grbcic (Grbčić et al., 2018) . As it is well known, in the case of linear isotropic classical elasticity problems, the boundary element method (BEM) is an alternative to the FEM. The main advantage of this method is the reduction by one of the dimension of the problem. It has already been successful for the solution of 2D micropolar elasticity problem. Sládek brothers derived the fundamental solutions and the associated traction for 3D isotropic micropolar elasticity problems (Sládek and Sládek, 1983). For anisotropic solids, the BEM could still be applied, but its main advantage which is the reduction of the problem dimension by one would be lost because the integral formulation will contain domain integrals. In recent years, a large number of researchers have invested in the development of the so-called meshless or meshfree methods. Among the various meshless approaches, the local point interpolation method is highly appealing on account of how simple it is to implement. This approach falls in accuracy in the presence of Neumann boundary conditions, which are almost an inevitability when solving solid mechanic problems. Liu *et al.* (Liu and Gu, 2001) have suggested a way to circumvent this difficulty by adopting the "weak-strong-form local point interpolation" method. Recently, Kouitat (Kouitat Njiwa, 2011a) introduced a novel numerical approach which combines the bests of the BEM and the local point interpolation method. The method called the LPI-BEM (Local Point Interpolation-Boundary Element Method) has already proven effective for the solution of various problems (e.g. (Schwartz et al., 2012; Thurieau et al., 2012, 2014)

This paper will discuss the effectiveness of the LPI-BEM method for solving 3D isotropic micropolar elasticity problems. The extension of the approach to deal with nonhomogeneous and/or anisotropic solids is straightforward. At first we will discuss the method and then we will validate this description by comparing the outputs of the specifically developed tool to literature results. Finally, the response of micropolar elastic solid to indentation load will be analyzed.

2- Governing Equations and method of solution

2-1. Governing equations

Following Eringen (Eringen, 1999a), in the theory of micropolar medium occupying the domain Ω with boundary Γ, the material point x is attached to a triad of directors that can rotate. Thus, the material point possesses six degrees of freedom: three degrees for the traditional translation (displacement) vector and three degrees for the micro-rotation vector. The field equations of

such a medium under quasi-static evolution without external body load are: (Iesan and Pompei, 1995), (Eringen, 1999a; Park and Lakes, 1986):

$$\sigma_{ji,j}(x) = 0 \quad (1)$$
$$m_{ji,j}(x) + \epsilon_{ijk}\sigma_{jk}(x) = 0 \quad (2)$$

In these equations, $\sigma_{ij}(x)$ represents the stress tensor and $m_{ij}(x)$ the moment stress tensor also called coupled-stress tensor.

With n_j as the outward normal vector on the boundary, the macro traction and the micro-torque acting at a regular point on the boundary are given respectively by:

$$t_i = \sigma_{ji}n_j\,, \qquad m_i = m_{ji}n_j \quad (3)$$

In the case of homogeneous centro-symmetric linear isotropic material, the constitutive relations are well documented and read:

$$\sigma_{ij} = \lambda\,\varepsilon_{rr}\delta_{ij} + 2(\mu+\kappa)\varepsilon_{ij} - \kappa\,u_{i,j} + \kappa\,\epsilon_{ijk}\varphi_k \quad (4)$$
$$m_{ij} = \alpha\,\omega_{rr}\delta_{ij} + (\beta+\gamma)\omega_{ij} + (\beta-\gamma)(\varphi_{i,j} - \varphi_{j,i})/2 \quad (5)$$

The fields ε_{ij} and ω_{ij} in these relations are expressed in terms of displacement $(u)$and microrotation (φ) gradients as:

$$\varepsilon_{ij} = (u_{i,j} + u_{j,i})/2$$
$$\omega_{ij} = (\varphi_{i,j} + \varphi_{j,i})/2$$

Parameters λ and μ are the Lamé constants and α, β, γ and κ are the micropolar constants.
The consideration of stability of the thermodynamic state, which in the static case requires that the strain energy is positive, has led to the following constraints on the parameters ((Eringen, 1999a)page 112)

$$3\lambda + 2\mu + \kappa \geq 0 \qquad 2\mu + \kappa \geq 0 \qquad \kappa = 0 \qquad 3\alpha + \beta + \gamma \geq 0$$
$$\beta + \gamma = 0 \qquad \gamma - \beta \geq 0$$

2-2 Solution Method

We aim to solve the problem of the static deformation of a micropolar solid by a boundary element based method. Let us remind the reader that, in the case of linear problems with well-established analytical fundamental solutions, the boundary element method has proven highly efficient (see e.g.(Balaš et al., 1989; Bonnet, 1999; Brebbia and Dominguez, 1996). In the case of the field equations we are dealing with, to our knowledge, no such fundamental solution exists for the three dimensional case. Let us point out that fundamental solution and associated traction have been derived for the plane strain case (e.g. (Atroshchenko et al., 2017; Liang and Huang, 1996; Shmoylova et al., 2007)). The 3D-problem can still be solved by the boundary element method, which is no longer pure since the formulation involves domain integrals and the main appeal of the approach (reduction of the problem dimension by one) is tarnished. This

shortcoming can be ruled out by adopting one of the strategies of conversion of domain integrals into boundary ones such as the dual reciprocity method (DRM)((Nardini and Brebbia, 1983) or radial integration method (RIM)((Gao, 2002). In recent years, a large number of researchers have invested in the development of so-called meshless or meshfree methods. Among the various meshless approaches, the local point interpolation method is highly appealing of how simple it is to implement. This approach falls in accuracy in the presence of Neumann type boundary conditions, which are almost an inevitability when solving solid mechanic problems. (LIU and GU, 2001) have suggested a way to circumvent this difficulty by adopting the "weak-strong-form local point interpolation" method. In a recent paper, (Kouitat Njiwa, 2011b) proposed a novel strategy that combines the best elements of both the conventional BEM and local point interpolation methods. This LPI-BEM approach has proved efficient in the context of anisotropic elasticity (Kouitat Njiwa, 2011b), piezoelectricity solids (Thurieau et al., 2012), multi-fields problems (Thurieau et al., 2014), and nonlocal elasticity (Schwartz et al., 2012). We adopted this method in our study, detailing below the principal steps followed in the context of a micropolar medium. First, let us introduce the following fictitious shear modulus and Poisson ratios.

$$\bar{G}_u = \mu + \kappa;\ \ \tilde{\nu}_u = \frac{\lambda}{2(\lambda+\mu+\kappa)};\ \ \bar{G}_\varphi = \frac{1}{2}(\gamma+\beta);\ \ \tilde{\nu}_\varphi = \frac{\alpha}{\beta+\gamma+2\alpha}$$

Note that we could equally adopt the usual shear modulus of micropolar material defined as $\bar{G}_u = \mu + \kappa/2$.

The field equations (1) and (2) take the forms:

$$\bar{G}_u\left[\Delta u_i + \frac{1}{1-2\tilde{\nu}_u}u_{j,ji}\right] - \kappa\, u_{j,ji} - \kappa\,\epsilon_{ijk}\varphi_{k,j} = 0 \tag{6}$$

$$\bar{G}_\varphi\left[\Delta\varphi_i + \frac{1}{1-2\tilde{\nu}_\varphi}\varphi_{j,ji}\right] + (\beta-\gamma)\frac{(\varphi_{j,ij}-\varphi_{i,jj})}{2} + 2\kappa\varphi_i + \kappa\,\epsilon_{ijk}u_{k,j} = 0 \tag{7}$$

Let us assume that the primary kinematical fields are the sum of a complementary part and a particular term. Namely: $u_i = u_i^c + u_i^p$ and $\varphi_i = \varphi_i^c + \varphi_i^p$. The complementary parts are assumed to satisfy Navier's type equations, that is:

$$\bar{G}_u\left[\Delta u_i^c + \frac{1}{1-2\tilde{\nu}_u}u_{j,ji}^c\right] = 0 \tag{8}$$

$$\bar{G}_\varphi\left[\Delta\varphi_i^c + \frac{1}{1-2\tilde{\nu}_\varphi}\varphi_{j,ji}^c\right] = 0 \tag{9}$$

and accordingly, the particular fields solve:

$$\bar{G}_u\left[\Delta u_i^P + \frac{1}{1-2\tilde{\nu}_u}u_{j,ji}^P\right] - \kappa\, u_{j,ji} - \kappa\,\epsilon_{ijk}\varphi_{k,j} = 0 \tag{10}$$

$$\bar{G}_\varphi\left[\Delta\varphi_i^P + \frac{1}{1-2\tilde{\nu}_\varphi}\varphi_{j,ji}^P\right] + (\beta-\gamma)\frac{(\varphi_{j,ij}-\varphi_{i,jj})}{2} + 2\kappa\varphi_i + \kappa\,\epsilon_{ijk}u_{k,j} = 0 \tag{11}$$

The Navier type equations 8 and 9 are solved by the conventional boundary element method which produces systems of equations of the following form (see e.g. (Balaš et al., 1989)):

$$[H_u]\{u^C\} = [G_u]\{t^C\}, \qquad [H_\varphi]\{\varphi^C\} = [G_\varphi]\{m^C\} \tag{12}$$

In equations (12), $\{u^C\}$, $\{\varphi^C\}$, $\{t^C\}$, $\{m^C\}$ represent respectively the vector of nodal displacement , the vector of nodal microrotation, the vector of nodal tractions and the vector of nodal micro-torque.

The local point interpolation, applied to the strong form differential equation, is adopted for the solution of equations (10) and (11).

In this method, a field v(x) is approximated as (LIU and GU, 2001): $v(x) = \sum_{i=1}^{N} R_i(r)a_i + \sum_{j=1}^{M} p_j(x)b_j$ with the following constraints: $\sum_{i=1}^{N} p_j(x)a_i = 0, j = 1 - M$ and $i = 1 - N$.

Here $R_i(r)$ is the selected radial basis functions, N the number of nodes in the neighborhood (support domain) of point x, and M the number of monomial terms in the selected polynomial basis $P_j(x)$. Recall that r denotes the Euclidean distance between the point x and the collocation center x^i. Enforcing the approximation of $v(x)$ to be satisfied at all centers in the support domain, coefficients a_i and b_j are determined by solving a system of equations of the form:

$$\begin{Bmatrix} v_{/L} \\ 0 \end{Bmatrix} = \begin{bmatrix} R & P \\ P^T & 0 \end{bmatrix} \begin{Bmatrix} a \\ b \end{Bmatrix}$$

where $\{v_{/L}\}$ denotes the vector of nodal values of $v(x)$.

It can be shown that $\{b\} = \left[[P]^T[R]^{-1}[P]\ \right]^{-1}[P]^T\,[R]^{-1}\{v_{/L}\} = [F_b]\{v_{/L}\}$ and $\{a\} = [R]^{-1}\left[[I] - [P]\,[F_b]\right]\{v_{/L}\} = [F_a]\{v_{/L}\}$.

Then, the approximation of $v(x)$ is now rewritten in the matrix form as $v(x) = [R_1 \quad R_2 \quad \ldots\ldots R_N]\,[F_a]\{v_{/L}\} + [P_1 \quad P_2 \quad \ldots\ldots P_m]\,[F_b]\{v_{/L}\}$

or more compactly as:

$$v(x) = [\Phi(x)]\{v_{/L}\} \tag{13}$$

In the matrix form, equations (10) and (11) become:

$$[B(\nabla)]^T[C_u][B(\nabla)]\{u^P\} + \nabla\nabla^T\{u\} + \kappa[D(\nabla)]\{\varphi\} = 0 \tag{14}$$

$$[B(\nabla)]^T[A_\varphi][B(\nabla)]\{\varphi^P\} + (\beta - \gamma)[\nabla\nabla^T + [I]\nabla^T\nabla]\{\varphi\} + \kappa\{\varphi\} - \kappa[D(\nabla)]\{u\} = 0 \tag{15}$$

In the above, $\{\nabla\} = \begin{pmatrix} \frac{\partial}{\partial x} & \frac{\partial}{\partial y} & \frac{\partial}{\partial z} \end{pmatrix}^T$, $\{z\} = (z_1 \quad z_2 \quad z_3)^T$, $[B(z)] = \begin{bmatrix} z_1 & 0 & 0 & z_2 & z_3 & 0 \\ 0 & z_2 & 0 & z_1 & 0 & z_3 \\ 0 & 0 & z_3 & 0 & z_1 & z_2 \end{bmatrix}^T$, $[D(\mathrm{z})] = \begin{bmatrix} 0 & -z_3 & z_2 \\ z_3 & 0 & -z_1 \\ -z_2 & z_1 & 0 \end{bmatrix}$ and $[I]$ is the identity tensor.

When adopting interpolation (13) for all kinematical fields, at a given collocation center, the particular fields equations (14) and (15) have become:

$$[B(\nabla)]^T[C_u][B(\nabla)]\big[\widetilde{\Phi}\big]\{u_{/L}^P\} + \kappa\big[\widetilde{\Phi}_1\big]\{u_{/L}\} + \kappa\big[\widetilde{\Phi}_2\big]\{\varphi_{/L}\} = \{0\} \tag{16}$$

$$[B(\nabla)]^T\big[A_\varphi\big][B(\nabla)]\big[\widetilde{\Phi}\big]\{\varphi_{/L}^P\} + \kappa\big[\widehat{\Phi}_0\big]\{\varphi_{/L}\} + (\beta-\gamma)\big[\widehat{\Phi}_1\big]\{\varphi_{/L}\} + \kappa\big[\widehat{\Phi}_3\big]\{u_{/L}\} = \{0\} \tag{17}$$

Matrices C_u and A_φ are the Voigt representation of the isotropic like elasticity tensor respectively with parameters $\bar{G}_u$ and $\tilde{\nu}_u$ n the one hand and $\bar{G}_\varphi$ and $\tilde{\nu}_\varphi$ on the other.

On collocation of the above equations (16) and (17) for all the internal collocation centers, taking the assumption that the particular integrals are identically zero at all boundary points, the following forms of systems of equations is obtained:

$$\{u^P\} = [A_u]\{u\} + [B_u]\{\varphi\} \tag{18}$$

$$\{\varphi^P\} = \big[A_\varphi\big]\{\varphi\} + \big[B_\varphi\big]\{u\} \tag{19}$$

The tractions at a regular point on the boundary is written as:

$$t_i = t_i^C + t_i^P + \delta t_i \text{ with } t_i^A = \big(\lambda\,\varepsilon_{rr}^A\delta_{ij} + 2(\mu+\kappa)\varepsilon_{ij}^A\big)n_j \quad (A = C \text{ or } P) \text{ and } \delta t_i = \big(-\kappa\,u_{i,j} + \kappa\,\epsilon_{ijk}\varphi_k\big)n_j \tag{20}$$

$$m_i = m_i^C + m_i^P + \delta m_i \text{ with } t_i^A = \big(\alpha\,\omega_{rr}^A\delta_{ij} + (\beta+\gamma)\omega_{ij}^A\big)n_j \quad (A = C \text{ or } P) \text{ and } \delta m_i = (\beta-\gamma)\big(\varphi_{j,i} - \varphi_{i,j}\big)n_j/2 \tag{21}$$

Following a similar strategy, the tractions at the boundary points could be written in the following forms:

$$\{t\} = \{t^c\} + [AK_{1u}]\{u^P\} + [AK_{uu}]\{u\} + \big[AK_{u\varphi}\big]\{\varphi\} \tag{22}$$

$$\{m\} = \{m^c\} + \big[AK_{1\varphi}\big]\{\varphi^P\} + \big[AK_{\varphi u}\big]\{u\} + \big[AK_{\varphi\varphi}\big]\{\varphi\} \tag{23}$$

Introduce equations (18) and (19) in (22) and (23), considering the previous consideration $u^c = u - u^P$ that we introduce in the system of equations (12) and after conducting some algebraic manipulations, the final coupled systems of equations is of the following forms:

$$[\bar{H}_u]\{u\} + \big[H_{u\varphi}\big]\{\varphi\} = [G_u]\{t\} \tag{24}$$

$$\big[\bar{H}_\varphi\big]\{\varphi\} + \big[H_{\varphi u}\big]\{u\} = \big[G_\varphi\big]\{m\} \tag{25}$$

Particularly worthy of mention, the final equations contained similar boundary primary variables and internal kinematic unknowns to those of a pure BEM. Boundary conditions could be taken into account as in standard practice and the resulting system of equations was solved by a standard direct solver.

3- Numerical examples

In our work, we used the generalized multi-quadrics radial basis functions $R_i(r) = \left(r_i^2 + c^2\right)^q$, where $r_i = \|x - x_i\|$ and c and q are parameters known as shape parameters. Shape parameter c was taken proportional to the minimum distance d_0, defined as the maximum value among the minimum distances in the x_1, $x_2$and x_3 directions between collocation centers.

The first set of numerical results presented serve as validation of the proposed numerical approach.

3.1 Case of a bar under traction load

Let us first consider the case of a bar under a uniform tension load ($\sigma_{33} = cte$). The bar with height H = 5 units has a rectangular cross section with width L =2 and thickness T = 1 units. (cf. fig 1). The bar is simply supported at its lower end and uniformly loaded at its upper face. All the remaining faces are free of traction. It is also assumed that all boundaries are free of micro-torque. The boundary of the bar was subdivided into 88 nine-node quadrilaterals. The boundary nodes were supplemented by 171 internal collocation centers. This case serves as a first validation of the developed numerical approach.

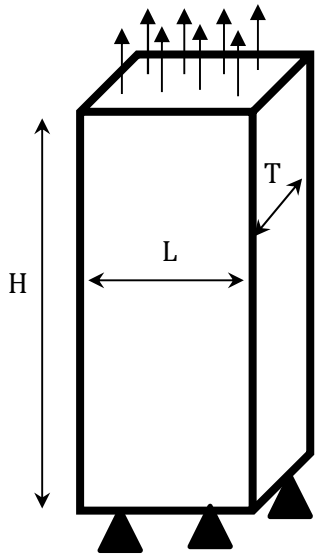

Figure 1 : Schematic of the bar under tension load

In this case, it can be established that, the axial strain is given in term of the applied traction by:

$$\varepsilon_{33} = \frac{2\lambda+2\mu_m+\kappa}{(3\lambda+2\mu_m+\kappa)(2\mu_m+\kappa)}\sigma_{33}$$

were $\mu_m = \mu + \frac{\kappa}{2}$ is the equivalent shear modulus for micropolar media and μ the Lamé constant. For our case, parameters are chosen as: $\lambda = 1000\ MPa$, $\mu_m = 750\ MPa$ and $\kappa = 500\ MPa$.

The calculated axial elongation along the central line of the sample is compared to the analytical solution in fig 2. As can be observed accurate numerical results are obtained. As expected, the calculated microrotation was identically zero. Indeed, due to the sample geometry, the loading does note generate shear stress. These results were undisturbed when the radial basis shape parameters were varied in the ranges $q \in [0.5; 2.5]$ and $c \in [10^{-4}d_0; 10^{-1}d_0]$.

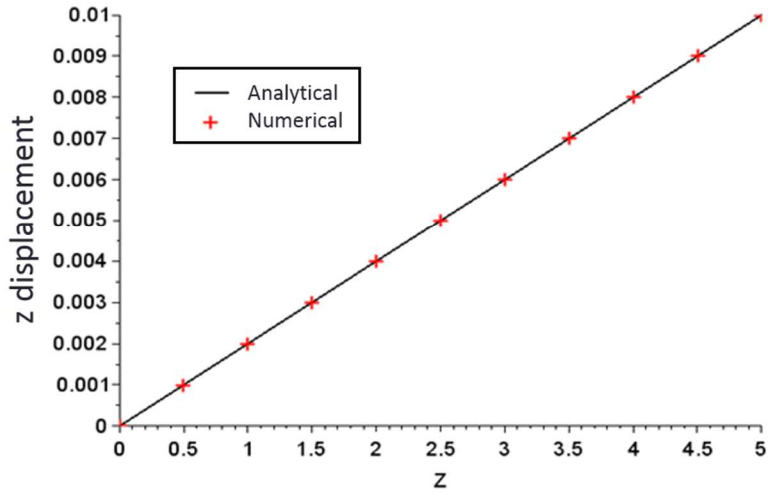

Figure 2: Axial displacement along the axial direction at the center of the beam

3.2 Complex loading of a prismatic bar

Case of a prismatic bar in order to further validate the developed numerical tool, let us consider the following patch tests used in (Grbčić et al., 2018). in order to validate their finite element implementation for elastic micropolar materials. The displacement and micro-rotation fields in a loaded prismatic bar with height H = 0.24, width L = 0.12 and thickness T=0.06, as shown in figure 3, are known. The adopted system of Cartesian coordinates is such that $0 \leq x \leq H$, $0 \leq y \leq T$, $0 \leq z \leq L$. The known fields are given by:

$$U_x = (x + 0.5y + z).10^{-3} \qquad U_y = (x + y + 0.5z).10^{-3} \qquad U_z = (0.5x + y + z).10^{-3}$$

$$\varphi_x = \varphi_y = \varphi_z = 0.25.10^{-3}$$

The stress field associated with such displacement and micro-rotation fields are given by:

$$\sigma_{xx} = \sigma_{yy} = \sigma_{zz} = 5$$
$$\sigma_{xy} = \sigma_{yz} = \sigma_{yz} = \sigma_{zy} = \sigma_{xz} = \sigma_{zx} = 1.5$$

The micro-stress is identically zero.

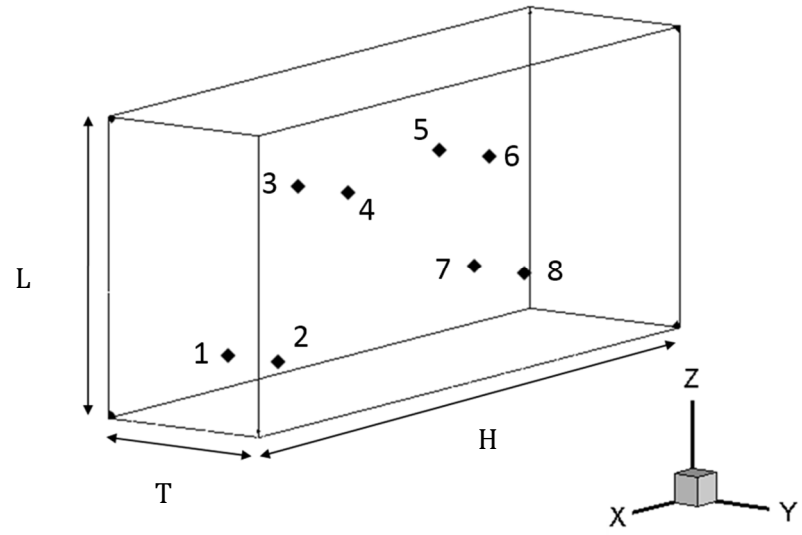

Figure 3 : Representation of the distribution of the collocation center in the considering medium

For our calculation each face of the sample is considered as a nine-node quadrilateral element. The boundary nodes are supplemented by 8 internal collocation centers shown in the figure.

Numerical results of our calculation are collected in the table below for all the internal 8 points:

	(x, y, z)	σ_{yy}	σ_{xz}	m_{xx}	m_{zx}
1	(0.04,0.02,0.02)	4.9984	1.5000	3.4445E-06	1.7422E-06
2	(0.04,0.04,0.02)	4.9986	1.4999	2.7052E-06	1.9378E-06
3	(0.08,0.02,0.08)	4.9943	1.4990	-1.7573E-06	-1.3079E-06
4	(0.08,0.04,0.08)	4.9939	1.4986	-1.5173E-06	-1.2852E-06
5	(0.16,0.02,0.08)	4.9947	1.4984	-8.3675E-08	1.0612E-06
6	(0.16,0.04,0.08)	4.9956	1.4988	-2.3694E-07	1.0647E-06
7	(0.18,0.02,0.03)	4.9968	1.4993	1.7310E-07	-1.8554E-06
8	(0.18,0.04,0.03)	4.9960	1.4992	1.9306E-07	-1.6577E-06

table 1: Stresses and micro-stresses at various points in the sample

As can be observed, results of our numerical tool are in excellent agreement with analytical solution. It can be concluded that our approach passed the test.

3.3 Torsion of a cylindrical specimen

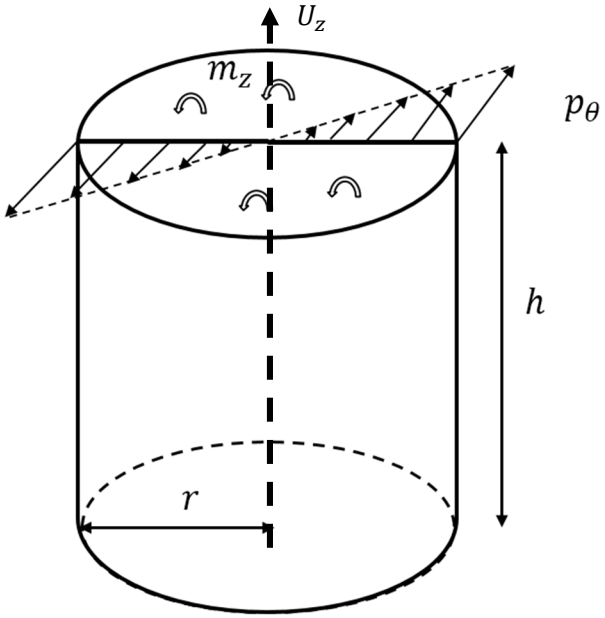

Figure 4 : cylinder in torsion

We now consider a cylindrical specimen subjected to torsion load as shown in figure 4. With this example we check the ability of the approach to deal with curved boundaries and natural boundary conditions. Let us remind the reader that this case has been considered in a recent work by Grbčić et al in a finite element context (Grbčić et al., 2018). They also derived the corresponding analytical solution which is used here for comparison purposes. The boundary of the cylinder with height $1\ mm$ and radius $0.2\ mm$ is subdivided into 96 nine-node quadrilateral elements. The boundary nodes were supplemented by 567 internal collocation centers. As shown in figure 4, each radius of the upper face of the cylinder is subjected to a linearly varying tangential traction ($p_\theta = 43.93\, r\ MPa\ with\ 0 \leq r \leq R$) simulating torsion. Each point of this upper face is subjected to a constant microtorque around the z-axis ($m_z = 3.64\ N.mm^{-1}$). The lower face of the sample is constrained against displacements and microrotation. The remaining face of the cylinder is free of traction and microtorque. As in the work of Grbčić et al. we used the following material parameters: λ=157 500 MPa, μ_m=8 750 MPa, κ=3 500 MPa, α=β=0 et γ=210 N.

The tangential displacement along a radius of the top surface and the microrotation along a cylinder generator are compared to the analytical solution in table 2 and 3.

r	U_θ numerical ($\times 10^{-3}$)	U_θ analytical ($\times 10^{-3}$)
0	0	0
0.025	0.4360	0.4330
0.05	0.8750	0.8660
0.075	1.3146	1.2989
0.1	1.7541	1.7318
0.125	2.1909	2.1678
0.15	2.6246	2.5977
0.175	3.0566	3.0307
0.1938	3.3806	3.3563

table 2: Data of displacements u_θ along the radius r on the upper face

And if we want to obtain values with more precision for the microstructure, it is necessary to refine the internal mesh.

z	φ_z numerical ($\times 10^{-2}$)	φ_z analytical ($\times 10^{-2}$)
0.0312	0.0500	0.0540
0.125	0.2161	0.2165
0.25	0.4305	0.4330
0.375	0.6644	0.6494
0.5	0.8939	0.8659
0.625	1.0926	1.0824
0.75	1.2820	1.2989
0.875	1.5166	1.5153
0.9688	1.6693	1.6778

table 3: Representation of microrotations φ_z along z on the lateral face

In the case of tangential displacement, the maximum relative error between computed and analytical results is less than 1.5%. In the case of microrotation, the maximum relative error (7%) is obtained near the constrained end. The further we get from this area, the smaller the relative error (less than 1.5%). It can be concluded that numerical results are in good agreement with analytical solutions.

As can be observed, in this case also sour numerical results are in excellent agreement with analytical prediction.

3.5 Case of a plate with a hole

Let us consider a plate with a hole as shown in figure 5a. This could represent a bone plate pierced to receive a screw. The plate has length 300 mm, width 200 mm and thickness 5 mm. The plate is loaded uniformly in the x direction. Due to symmetry, only a quarter of the specimen is considered for calculation (fig 5b).

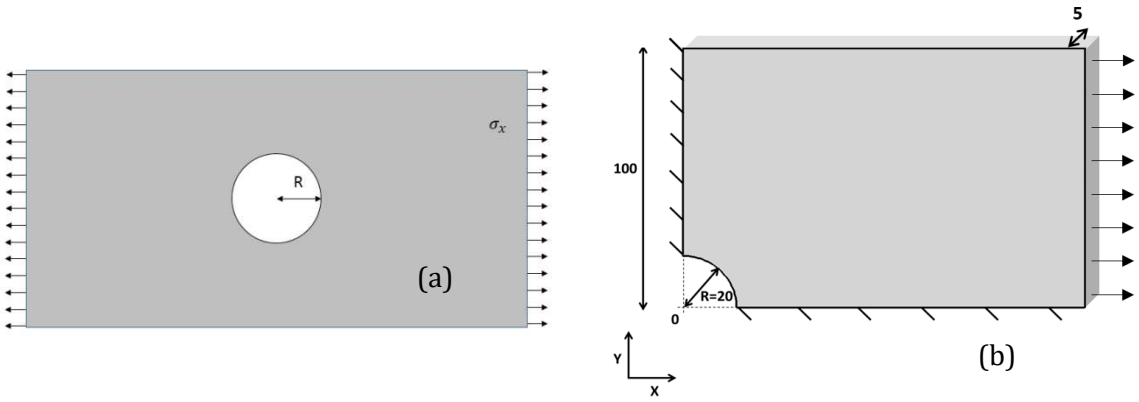

Figure 5 : quater of aplate with a central circular hole of radius R

Following, symmetry boundary conditions are applied at the left and the bottom ends of the geometry, the hole surface and the upper and lower faces of the plate are free of traction. Microrotations are zero at the left and the bottom ends while the microtorques are zero at the remaining surfaces. This example has already been considered by Eringen (Eringen, 1999b) and Rosenberg (Rosenberg and Cimrman, 2003). They introduced a characteristic length of the material defined as $c = \left(\frac{\gamma(\mu+\kappa)}{\kappa(2\mu+\kappa)}\right)^{1/2}$ analyzed they results with respect to the ratio R/c where R is the hole radius. . The macroscopic material parameters (λ and μ) adopted for each value of the ratio R/c are determined by considering that $b = \left(\frac{\gamma}{2(2\mu+\kappa)}\right)^{1/2}$, γ =260 N and $R = 20\,mm$. We take $b/c = 0.4$ and $\upsilon = 0.2 = \lambda/(2\lambda + 2\mu + \kappa)$.

Results from our simulations are analyzed through the evolution of the maximum tangential stress – the stress intensity factor – generated in the hole with respect to the ratio R/c. This evolution is shown in the plot in figure 6 where it is compared to the case of a pure elastic material. The results, which agree well with those of Eringen (Eringen, 1999b) and Rosenberg (Rosenberg and Cimrman, 2003) show that the stress intensity factor gently increases through the pure elastic value as the material length scale decreases.

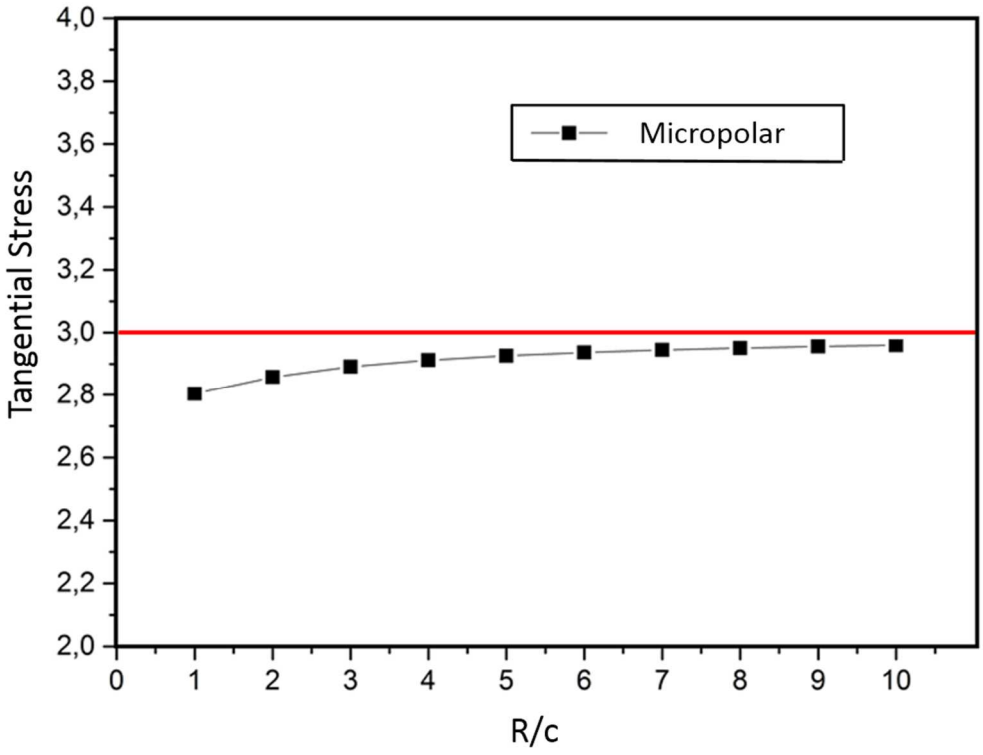

Figure 6: Maximum tangent stress in the hole (on the x direction)

It is observed that the smaller this characteristic length c the closer we get to the elastic case.

Now let's look at the micro rotation. The presence of the hole induces shear stresses which do not exist in a plate without hole (cf exemple 1).

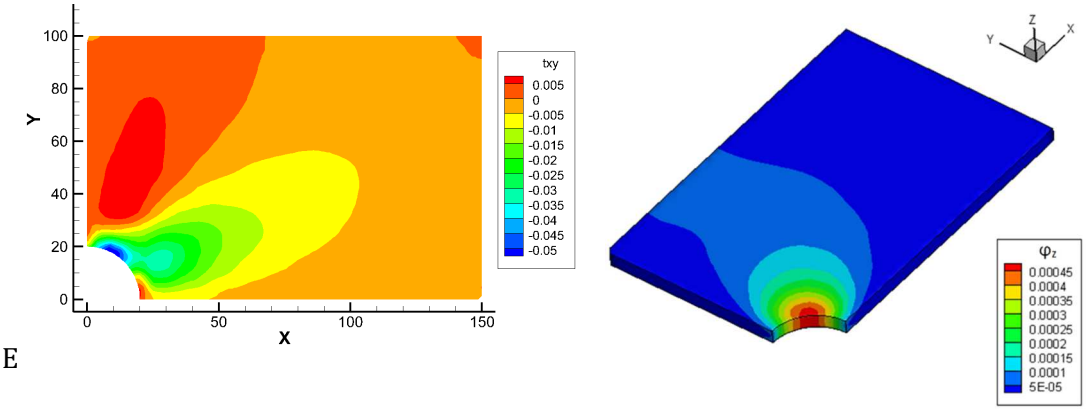

E

Figure 7: Representation of the - (a) tangent stress t_{xy} - (b) microrotation φ_z in the hole plate

The shear stresses in this case are maximum at the edge of the hole and they induce a noticeable micro-rotations in the same place.

3.5 Localized load on a micropolar sample simulating indentation load

In this example we will simulate an indentation by a spherical punch of a cubic homogeneous and isotropic specimen. To do this we will assume that the displacement profile under the

indenter is similar to the one obtained when indenting a pure elastic sample. The expression of this displacement is known and can be find in the book by KL Johnson (Johnson, 1987).

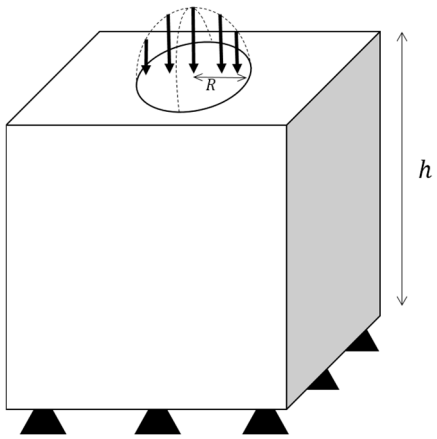

Figure 8: Representation of the domain with boundary

In our application, the cubic sample has size $h = 10$ mm and the non-deformable spherical punch has radius $R_{ind} = 10$ mm. Under a normal applied load P, the normal displacement beneath the indenter is given by $U_z(r) = U_z(0) * (1 - \left(\frac{r}{2a}\right)^2)$ where r stands for the position on a radius of the contact disc with radius a. $U_z(0)$ is the displacement of the first contact point (i.e. the center of the circular contact area). In the case of an elastic infinite flat specimen with Young modulus E and Poisson ratio ν, the mean pressure in the contact disc (P_m) is related to the maximum contact stress (P_0) by $P_m = \frac{2}{3}P_0$ with $P_o = \frac{2E^*a}{\pi R_{ind}}$. $E^*$is an equivalent modulus given by: $E^* = \frac{E}{1-\nu^2}$.

In the following, we compare the response of a pure elastic material to that of a micropolar one. Both materials are selected to have the same macroscopic material parameters collected in table 4 below.

	$E\ (GPa)$	ν	$\kappa\ (GPa)$	$\alpha\ (N)$	$\beta\ (N)$	$\gamma\ (N)$	N_c
Elastic case	85.2	0.36	/	/	/	/	/
Micropolar case	85.2	0.36	30	-50	50	260	0.57

table 4: material parameter for classical and micropolar elastic medium

In table 4 N_c is a coupling number for macro/microstructure (for micropolar media) defined as $N = \sqrt{\frac{\kappa(1+\nu)}{E+\kappa(1+\nu)}}$. N is a number that highlights the connectivity or the topology of the microtructure network, in other words it quantifies the degree of micropolarity exhibited by the material. A quadratic network microstructure should have a higher parameter than a hexagonal network microstructure and so on (McGregor and Wheel, 2014).

A first set of numerical experiment has been performed for different values of contact area radius (see table 5 below).

	Case 1	Case 2	Case 3	Case 4	Case 5	Case 6
$\frac{a}{h}$	0.025	0.05	0.075	0.1	0.125	0.15

table 5: Table summarizing the different cases according to the maximum insertion depths

The calculated maximum contact pressure (P_o) computed for the pure elastic material and the micropolar elastic material are compared to the pure elastic analytical solution in figure 11.

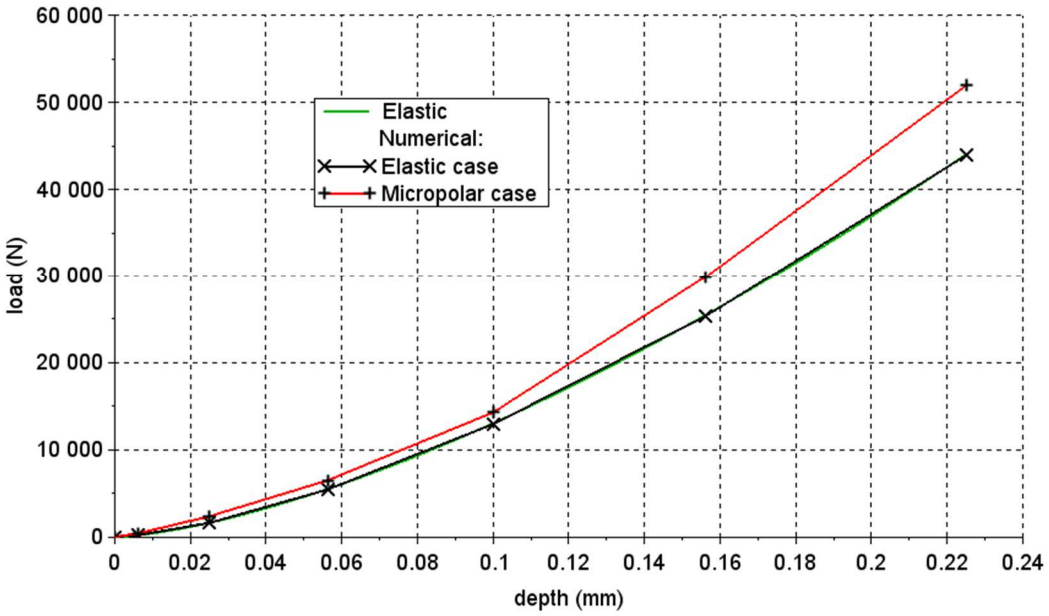

Figure 9: Representation of the indentation curves representing the penetration depth as a function of the applied load

It can be observed that our numerical solution is in excellent agreement with analytical one in the case of pure elastic material. Globally, the load required to achieve the same penetration depth (the same contact area) is higher in the case of micropolar material. This is in agreement with the results presented by (Salehi and Salehi, 2014).

Let us introduce s the stress tensor deviator define as $s = \sigma - \frac{1}{3}tr(\sigma) * I$, with σ the asymmetric stress tensor and m the micro-stress tensor. Due to the asymmetric stress tensor (Eringen, 1999c), we can't use the usual von Mises stresses definition for an elastic classical medium. An equivalent stress of the von Mises type has been introduced by Gombos (Gombos, 2007) and is given by:

$$\sigma_{vm} = \sqrt{3\left(\frac{1}{4}(s:s + s:s^t) + \frac{1}{4}(m:m + m:m^t)\right)}$$

This stress is considered in the analysis of results of the specimen submitted to indentation type loading.

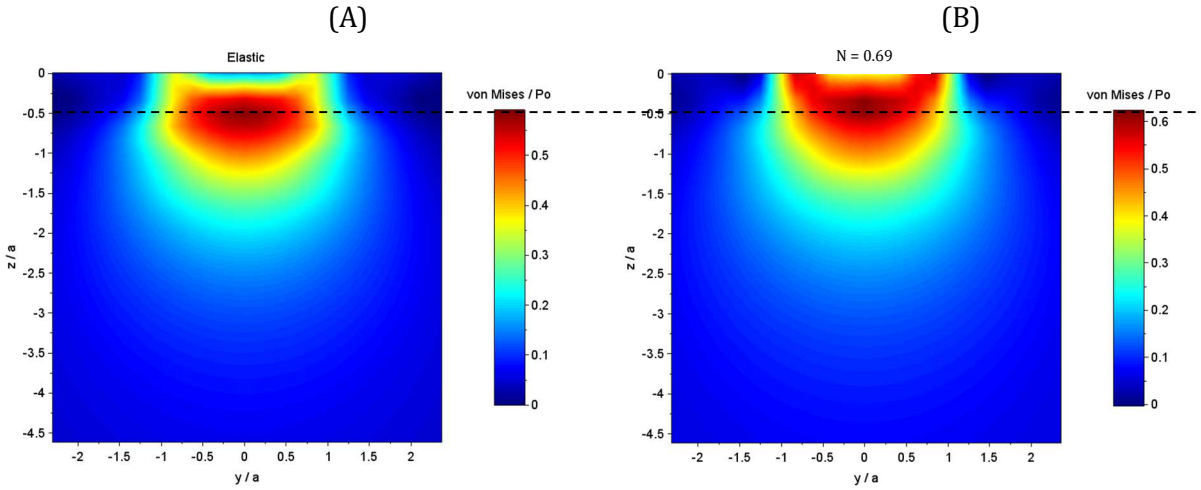

Figure 10: von Mises stress in a cross plane of the specimen (plane xy containing the symmetry axis) ; A) pure elastic material ; B) micropolar elastic material.

The contour plots of the von Mises stresses in a vertical plane containing the axis of symmetry are shown in figure 10. The purely elastic case is shown for comparison purpose. It can be noted that the subsurface stresses are higher in the case of micropolar elastic material. The maximum value is located on the symmetry axis but closer to the contact compared to the pure elastic case. Higher values of equivalent stresses are obtained at the free surface in a region enclosing the contact border.

Let us consider the effect of the coupling number N_c on the distribution of the normal stress and the stress within the sample. The different values of the coupling number have been obtained by modifying the value of parameter κ and the Young Modulus and Poisson coefficient stay the same.

The profiles of normal contact load within the contact are shown in figure 11 below.

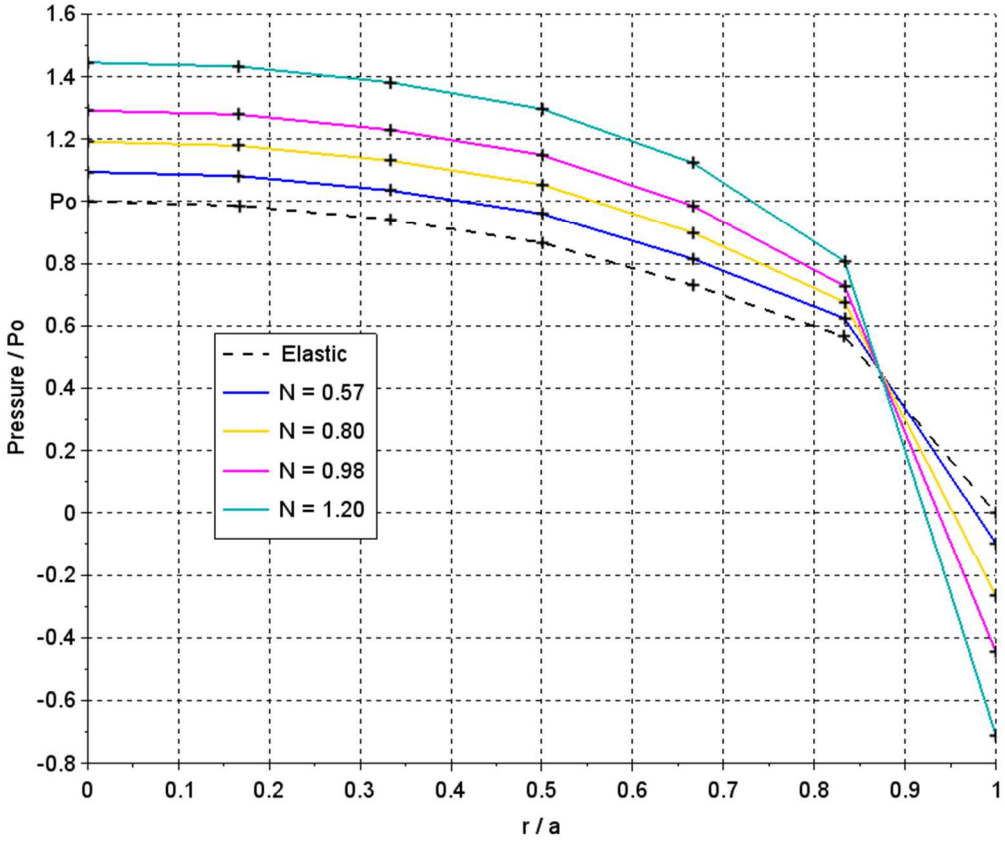

Figure 11: Representation of the constrained vector z dimensioned by p0 on the contact radius

Clearly, the higher the coupling number, the higher the values of the normal contact stress. This result indicates that, for a given normal load P applied on a spherical punch, the higher the degree of micropolarity, the smaller the radius of the contact area.

For a given radius of contact area, the contour plots of the von Mises stresses developed within the sample are shown in figure 12. The stress levels increase with the value of the coupling number. Moreover, the maximum value is obtained at the surface and in the material. For higher values of the coupling number, the maximum value is located at the surface of the sample. This is a clear difference with the case of classical elasticity

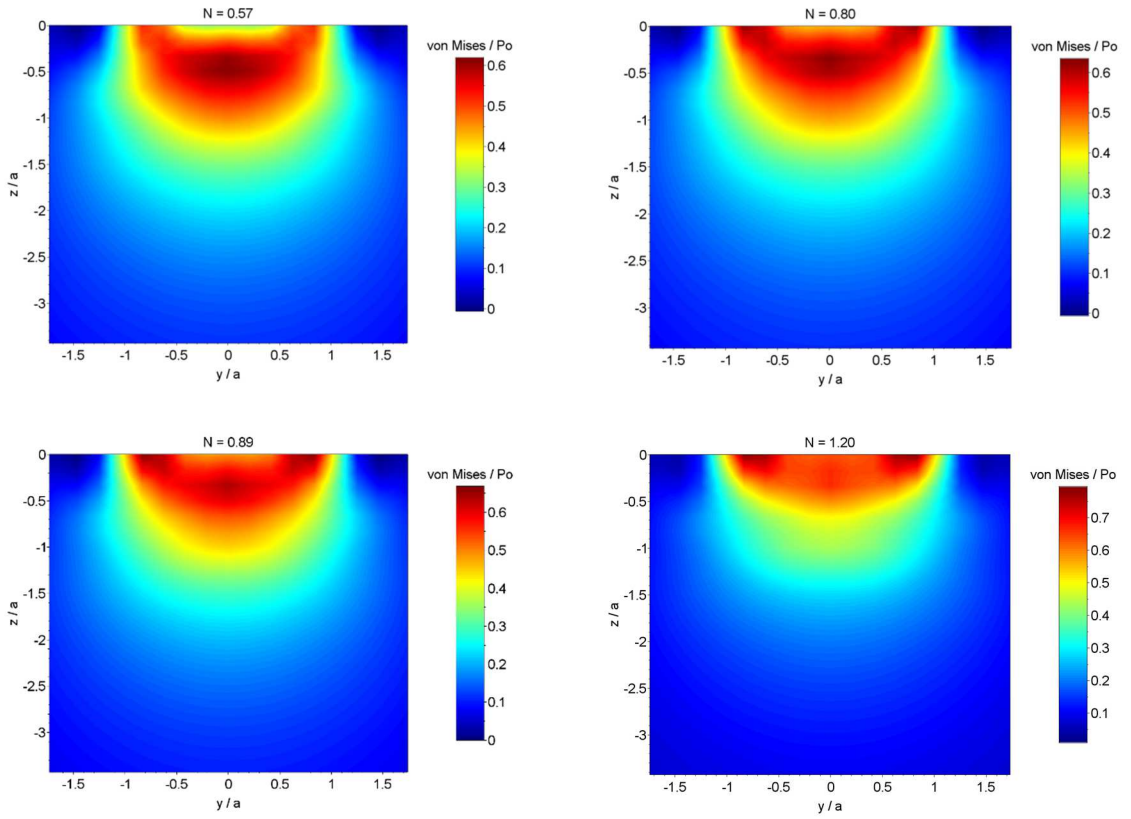

Figure 12: Representation of von Mises constraints in the xy plane passing through the center of the domain for the micropolar in function of the coupling number N

Conclusion

A pure boundary element method for the solution of 3D micropolar elasticity problems has been presented. The approach is the so-called LPI-BEM which combines the advantages of the boundary element method (reduction of the problem dimension by one) and of the local point interpolation method (ease of implementation). The effectiveness of the approach in this context has been proved by comparing our results with those available in the literature. The case of indentation has also been considered and some first results highlighted. A forthcoming will be dedicated to the indentation of micropolar elastic materials, focusing on the role of the known characteristic length and coupling number usually adopted for this material.

Bibliographies

Altenbach, H., and Eremeyev, V. a. (2009). On the linear theory of micropolar plates. ZAMM - J. Appl. Math. Mech. Z. Für Angew. Math. Mech. *89*, 242–256.

Atroshchenko, E., Hale, J.S., Videla, J.A., Potapenko, S., and Bordas, S.P.A. (2017). Micro-structured materials: Inhomogeneities and imperfect interfaces in plane micropolar elasticity, a boundary element approach. Eng. Anal. Bound. Elem. *83*, 195–203.

Balaš, J., Sládek, J., and Sládek, V. (1989). Stress analysis by boundary element methods (Amsterdam; New York: Elsevier).

Bonnet, M. (1999). Boundary Integral Equation Methods for Solids and Fluids. Meccanica *34*, 301–302.

Brebbia, C.A., and Dominguez, J. (1996). Boundary Elements: An Introductory Course (Sydney Grammar School Press).

Cosserat, E.M.P., and Cosserat, F. (1909). Théorie des corps déformables (Paris: A. Hermann et fils).

Diebels, S. (2000). A macroscopic description of the quasi-static behavior of granular materials based on the theory of porous media. Granul. Matter *2*, 143–152.

Diebels, S. (2002). Micropolar mixture models on the basis of the Theory of Porous Media. In Porous Media, P.D.-I.W. Ehlers, and P.D.D.-I.J. Bluhm, eds. (Springer Berlin Heidelberg), pp. 121–145.

Diepolder, W., Mannl, V., and Lippman, H. (1991). The cosserat continuum, a model for grain rotations in metals? Int. J. Plast. *7*, 313–328.

Eringen (1990). Electrodynamics of Continua I: Foundations and Solid Media.

Eringen, A.C. (1999a). Microcontinuum Field Theories (New York, NY: Springer New York).

Eringen, A.C. (1999b). Microcontinuum Field Theories I. Foundations and Solids (New York, NY: Springer New York).

Eringen, A.C. (1999c). Theory of Micropolar Elasticity. In Microcontinuum Field Theories, (Springer New York), pp. 101–248.

Gao, X.-W. (2002). The radial integration method for evaluation of domain integrals with boundary-only discretization. Eng. Anal. Bound. Elem. *26*, 905–916.

Goddard, J.D. (2008). From Granular Matter to Generalized Continuum. In Mathematical Models of Granular Matter, G. Capriz, P.M. Mariano, and P. Giovine, eds. (Springer Berlin Heidelberg), pp. 1–22.

Gombos, Á. (2007). Equivalent stress for micropolar solids. Period. Polytech. Mech. Eng. *51*.

Grbčić, S., Ibrahimbegović, A., and Jelenić, G. (2018). Variational formulation of micropolar elasticity using 3D hexahedral finite-element interpolation with incompatible modes. Comput. Struct. *205*, 1–14.

Green, A.E., Naghdi, P.M., and Wainwright, W.L. (1965). A general theory of a Cosserat surface. Arch. Ration. Mech. Anal. *20*, 287–308.

Iesan, D., and Pompei, A. (1995). On the equilibrium theory of microstretch elastic solids. Int. J. Eng. Sci. *33*, 399–410.

Johnson, K.L. (1987). Contact Mechanics (Cambridge University Press).

Kouitat Njiwa, R. (2011a). Isotropic-BEM coupled with a local point interpolation method for the solution of 3D-anisotropic elasticity problems. Eng. Anal. Bound. Elem. *35*, 611–615.

Kouitat Njiwa, R. (2011b). Isotropic-BEM coupled with a local point interpolation method for the solution of 3D-anisotropic elasticity problems. Eng. Anal. Bound. Elem. *35*, 611–615.

Lakes, R.S. (1986). Experimental microelasticity of two porous solids. Int. J. Solids Struct. *22*, 55–63.

Li, L., and Xie, S. (2004). Finite element method for linear micropolar elasticity and numerical study of some scale effects phenomena in MEMS. Int. J. Mech. Sci. *46*, 1571–1587.

Liang, K.-Z., and Huang, F.-Y. (1996). Boundary element method for micropolar elasticity. Int. J. Eng. Sci. *34*, 509–521.

Liu, G.R., and Gu, Y.T. (2001). A local radial point interpolation method (LRPIM) for free vibration analyses of 2-D solids. J. Sound Vib. *246*, 29–46.

LIU, G.R., and GU, Y.T. (2001). A LOCAL RADIAL POINT INTERPOLATION METHOD (LRPIM) FOR FREE VIBRATION ANALYSES OF 2-D SOLIDS. J. Sound Vib. *246*, 29–46.

McGregor, M., and Wheel, M.A. (2014). On the coupling number and characteristic length of micropolar media of differing topology. Proc. R. Soc. Math. Phys. Eng. Sci. *470*, 20140150.

Mindlin, R.D., and Tiersten, H.F. (1962). Effects of couple-stresses in linear elasticity. Arch. Ration. Mech. Anal. *11*, 415–448.

Nardini, D., and Brebbia, C.A. (1983). A new approach to free vibration analysis using boundary elements. Appl. Math. Model. *7*, 157–162.

Park, H.C., and Lakes, R.S. (1986). Cosserat micromechanics of human bone: Strain redistribution by a hydration sensitive constituent. J. Biomech. *19*, 385–397.

Ramezani, S., Naghdabadi, R., and Sohrabpour, S. (2008). Non-linear finite element implementation of micropolar hypo-elastic materials. Comput. Methods Appl. Mech. Eng. *197*, 4149–4159.

Ramezani, S., Naghdabadi, R., and Sohrabpour, S. (2009). Constitutive equations for micropolar hyper-elastic materials. Int. J. Solids Struct. *46*, 2765–2773.

Rosenberg, J., and Cimrman, R. (2003). Microcontinuum approach in biomechanical modeling. Math. Comput. Simul. *61*, 249–260.

Salehi, S.H., and Salehi, M. (2014). Finite element study for conical indentation of elastoplastic micropolar material. Int. J. Solids Struct. *51*, 3987–3995.

Schwartz, M., Niane, N.T., and Kouitat Njiwa, R. (2012). A simple solution method to 3D integral nonlocal elasticity: Isotropic-BEM coupled with strong form local radial point interpolation. Eng. Anal. Bound. Elem. *36*, 606–612.

Shmoylova, E., Potapenko, S., and Rothenburg, L. (2007). Boundary element analysis of stress distribution around a crack in plane micropolar elasticity. Int. J. Eng. Sci. *45*, 199–209.

Sládek, V., and Sládek, J. (1983). Boundary integral equation method in micropolar elasticity. Appl. Math. Model. *7*, 433–440.

464 Thurieau, N., Kouitat Njiwa, R., and Taghite, M. (2012). A simple solution procedure to 3D-
465 piezoelectric problems: Isotropic BEM coupled with a point collocation method. Eng. Anal.
466 Bound. Elem. *36*, 1513–1521.

467 Thurieau, N., Kouitat Njiwa, R., and Taghite, M. (2014). The local point interpolation–boundary
468 element method (LPI–BEM) applied to the solution of mechanical 3D problem of a
469 microdilatation medium. Eur. J. Mech. - ASolids *47*, 391–399.

470